

MIT Open Access Articles

*Magnetoelastic effects in $\text{SrTi}_{1-x}\text{M}_x\text{O}_3$
($M = \text{Fe}, \text{Co}, \text{or Cr}$) epitaxial thin films*

The MIT Faculty has made this article openly available. **Please share** how this access benefits you. Your story matters.

Citation: Kim, Dong et al. "Magnetoelastic effects in $\text{SrTi}_{1-x}\text{M}_x\text{O}_3$ ($M = \text{Fe}, \text{Co}, \text{or Cr}$) epitaxial thin films." *Physical Review B* 84 (2011): n. pag. Web. 17 Nov. 2011. © 2011 American Physical Society

As Published: <http://dx.doi.org/10.1103/PhysRevB.84.014416>

Publisher: American Physical Society

Persistent URL: <http://hdl.handle.net/1721.1/67051>

Version: Final published version: final published article, as it appeared in a journal, conference proceedings, or other formally published context

Terms of Use: Article is made available in accordance with the publisher's policy and may be subject to US copyright law. Please refer to the publisher's site for terms of use.



Magnetoelastic effects in $\text{SrTi}_{1-x}\text{M}_x\text{O}_3$ ($\text{M} = \text{Fe}, \text{Co}, \text{or Cr}$) epitaxial thin films

Dong Hun Kim, Lei Bi, Peng Jiang, Gerald F. Dionne, and C. A. Ross*

Department of Materials Science and Engineering, Massachusetts Institute of Technology, Cambridge, Massachusetts, USA

(Received 26 January 2011; revised manuscript received 6 May 2011; published 25 July 2011)

$\text{SrTi}_{1-x}\text{M}_x\text{O}_3$ films in which $\text{M} = \text{Fe}, \text{Co}, \text{or Cr}$ and $x = 0.04\text{--}0.5$ have been grown epitaxially on CeO_2 -buffered Si, SrTiO_3 , and LaAlO_3 substrates. Films grown in vacuum containing Fe or Co typically showed a strong uniaxial magnetic anisotropy in the out-of-plane direction, a saturation moment on the order of $0.5\mu_B/\text{Fe}$ or Co, and a magnetization that persists to temperatures of order 1000 K. In contrast, films containing Cr showed no evidence of a spontaneous magnetic moment. The films are typically in a high in-plane compressive strain state due to epitaxial growth. The results are discussed in terms of the magnetoelastic effects from specific ionic valence states, and the magnetization versus temperature curves are fitted to a model for magnetoelastic spin ordering.

DOI: [10.1103/PhysRevB.84.014416](https://doi.org/10.1103/PhysRevB.84.014416)

PACS number(s): 75.47.Lx, 75.30.Gw

I. INTRODUCTION

Stimulated by the discovery of room-temperature magnetism in TiO_2 thin films containing low Co concentrations,¹ numerous studies of transition metal-substituted oxides have been carried out for potential spintronic, magnetoelectronic, and optical applications.^{2–4} Although considerable effort has been made to account for the magnetism of dilute compounds, the origins of the high-temperature ferromagnetism are not understood completely. Some researchers have reported that defects and/or oxygen vacancies could be responsible for the ferromagnetism^{5,6} while other groups have suggested that “double” exchange between mixed-valence transition-metal ions is responsible for the magnetic properties.^{7,8} Dinia⁹ and Ryu¹⁰ proposed that the magnetism arises from heterogeneity or segregation of secondary ferromagnetic phases while other groups found no evidence of phase segregation.^{11,12} Coey *et al.* discussed a mechanism based on the exchange coupling of F-centers in a spin-split impurity band model.^{13,14}

Long-range spin ordering in transition metal-substituted oxides is a collective phenomenon that originates from local molecular (short-range) electron stabilization of the covalent bond formed by $3d\text{--}2p$ cation-anion orbital overlap integrals. As a consequence, long-range ordering above room temperature is unlikely to be obtained in dilute magnetic compounds. Moreover, in an oxide insulator, the hybrid ground state formed from the overlapping of two half-filled orbitals is a symmetric *bonding* state, which dictates that the spins should be stabilized antiferromagnetically to satisfy the Pauli principle.^{15–17}

One mechanism with energy sufficient to create magnetic ordering in the absence of exchange effects is magnetoelasticity, which is responsible for anisotropy and magnetostriction in ferrimagnetic oxides.^{17–19} Magnetoelastic effects are important in strained films, and have, for example, been used to account for the magnetic anisotropy in SrRuO_3 films on a SrTiO_3 substrate.^{20,21} We show here that the magnetoelastic effects from low or moderate concentrations of certain transition-metal ions can dominate the magnetic properties in strained epitaxial oxide films. We present magnetic and structural data from perovskite SrTiO_3 thin films with Fe, Co, and Cr substitution for Ti up to $\sim 50\%$, and interpret the strong anisotropy and non-Brillouin temperature dependence of magnetization in terms of magnetoelastic effects.

II. MAGNETOELASTICITY IN OCTAHEDRAL SITES

Studies of magnetism in oxides have historically focused on ferrimagnetic spinel and garnet compounds used for information storage and for various control devices for radar and other electromagnetic propagation systems. The main source of magnetism in these materials is the Fe^{3+} ($3d^5$, $t_{2g}^3e_g^2$) high-spin ion which has an orbital singlet ground state and lacks first-order orbital momentum.¹⁷ The absence of direct coupling between orbital-momentum states and the octahedrally symmetric crystal field reduces the magnetic anisotropy to a second-order effect, and makes magnetostriction a minor effect. However, other $3d^n$ ions have proven to be important design aids for controlling stress sensitivity and anisotropy. The Jahn-Teller effect of Mn^{3+} ($3d^4$) is useful in promoting square hysteresis loops with low coercivity, and the strong spin-orbit-lattice interactions of Co^{2+} ($3d^7$) can adjust anisotropy fields or enhance spin-lattice relaxation rates at radio frequencies.²²

In Fig. 1(a), the origin of the magnetoelastic properties that produce a tensile strain along the z axis is illustrated by the d^n -electron Aufbau diagrams for the most common high-spin cases d^4 , d^6 , and d^7 . With degenerate orbital ground states, all three configurations can cause spontaneous [001] z -axis distortions of the octahedral-site ligands to lower the net electronic energy of the spin configuration by splitting the orbital t_{2g} or e_g degeneracy. The distortion can be an expansion (+) or contraction (–) resulting in a ground doublet $d_{\pm 1}$ [$= (1/\sqrt{2})(d_{xz} \pm id_{yz})$] or singlet d_{xy} , respectively. There is an important distinction between stabilization occurring in the e_g or t_{2g} shell. For example, Mn^{3+} stabilizes its sole electron in the e_g states by a z -axis expansion through direct orbit-lattice interaction [see Fig. 1(a), d^4 case]. However, Fe^{2+} (d^6) and Co^{2+} (d^7) provide stabilized spins in the t_{2g} shell where unquenched orbital momentum is present in the unstressed state and leaves an orbital triplet and a spin-orbit coupling multiplet group.^{23,24} In Fig. 1(b), Aufbau diagrams are presented for d^4 , d^5 , and d^6 cases in low-spin configurations. These situations arise when the crystal-field splitting $10Dq$ between the e_g and t_{2g} levels is great enough to overcome the Hund’s rule stabilization energy U_{ex} for maximum spin in the ground state, and instead allows the t_{2g} states to fill with paired spins. In some cases, remaining degeneracies leave a spin-orbit doublet to create further stabilization of an unpaired spin. In general,

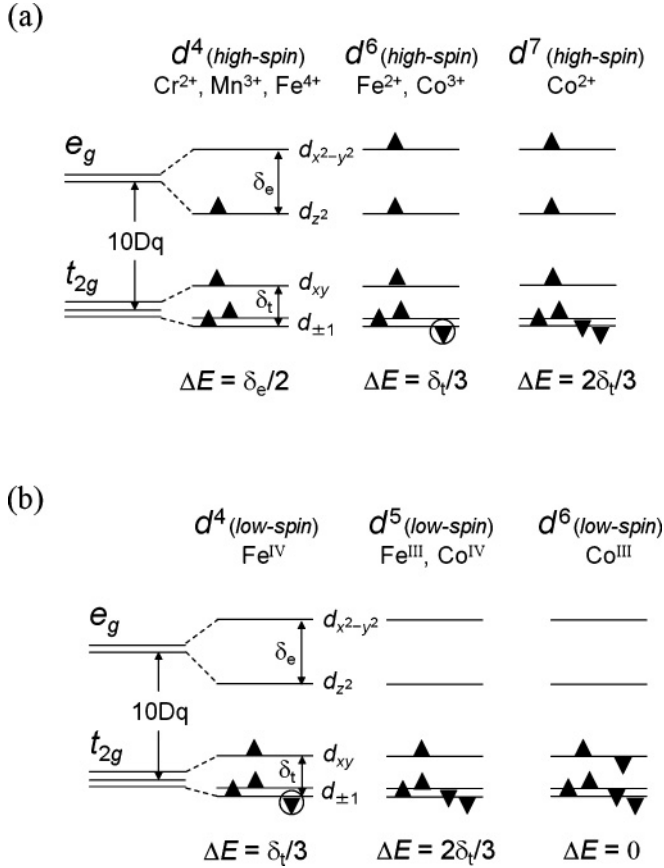


FIG. 1. Selected one-electron (Aufbau) diagrams for d^4 , d^5 , d^6 , and d^7 ions in an octahedral site with z -axis tetragonal expansion (circles indicate spin-orbit degeneracy): (a) high-spin states with all spins aligned according to Hund's rule. In d^4 , there is a stabilization of an electron spin by the splitting of the e_g orbital degeneracy without spin-orbit coupling influence (J-T effect). In d^6 an orbital degeneracy remains in the surviving doublet of the t_{2g} term, which will be stabilized as the ground state (preferred), depending on whether the strain leads to expansion or contraction of the octahedron, and (b) low-spin configurations in violation of Hund's rule in a z -axis expansion where all spins occupy the degenerate t_{2g} orbital. This condition can be expected in higher valence states, greater than 3+. Here, d^5 is included because it is now magnetoelastic with a single unpaired spin; d^6 is no longer stabilized by the distortion because the t_{2g} states are filled. δ_t and δ_e are defined in eq. (1) and ΔE represents the corresponding energy stabilization.

low-spin configurations can be expected in 4+ valence states (or higher) where the crystal-field energy is large, i.e., $10Dq > U_{ex}$.²⁵ Table I presents a summary of transition-metal ion electronic structures and their expected magnetoelastic effects. Sensitivity of the magnetic properties to the strain state of a material is expected from certain octahedrally coordinated ions, specifically Cr^{2+} , Mn^{3+} , Fe^{4+} , Fe^{2+} , Co^{2+} , Co^{3+} , Co^{4+} , Ni^{3+} , and Cu^{2+} (high-spin), and Fe^{IV} , Fe^{III} , and Co^{IV} (low-spin). On the contrary, no magnetoelastic effects are expected from other common ions such as Cr^{3+} , Ni^{2+} , and Fe^{3+} in octahedral sites because they stabilize ground-state singlets.

Several characteristic behaviors are expected in materials that are dominated by magnetoelastic (ME) effects. The material can exhibit magnetic anisotropy even for low concentrations of dopant where exchange interactions are insignificant. In a biaxially stressed thin film, the anisotropy will be in plane or out of plane depending on the signs of the stress and the magnetoelastic (or magnetostriction) constants. For Jahn-Teller singlet stabilization, we expect a positive out-of-plane magnetoelastic constant (i.e., the easy axis aligns perpendicular to the film plane for a (100) film with compressive in-plane or tensile out-of-plane strain), and a negative magnetoelastic constant for a spin-orbit (S-O) doublet ground state.¹⁷ For epitaxial films, the anisotropy will depend on the film/substrate lattice mismatch and anisotropy fields can be several kOe. The magnetization can persist to well above room temperature but the $M(T)$ curve does not follow the convex Brillouin contour characteristic of exchange-dominated systems.^{26,27} Additionally, the saturation magnetization does not rise in direct proportion to the amount of transition metal in the lattice and can decrease with higher concentration due to antiferromagnetic exchange between nearest neighbors.

These features of ME-dominated systems are inconsistent with the presence of metallic clusters, which give no anisotropy, a size-dependent blocking temperature above which superparamagnetism occurs, and an increase in saturation magnetization with concentration. These features are also inconsistent with systems dominated by exchange, which differ in their anisotropy field and $M(T)$ characteristic. Indeed, the presence of anisotropy even for systems with low percentages of transition metals is a good indication that ME effects are important.

In the following sections, magnetoelastic effects are examined in a diamagnetic host oxide $SrTiO_3$ in which Fe, Co, and Cr are substituted on the Ti sites, and the results are discussed in the context of magnetoelastic effects. We consider the case where the concentrations of substituents are raised above dilute levels but kept below $\sim 50\%$. Other examples of oxide compounds containing magnetoelastic ions are listed in Ref. 26.

III. EXPERIMENTAL METHODS

The perovskite films were deposited by pulsed laser deposition (PLD) using a KrF excimer laser ($\lambda = 248$ nm). 1-inch diameter targets of yttria-stabilized zirconia (YSZ), CeO_2 , $SrTiO_3$ (STO), $Sr(Ti_{1-x}Fe_x)O_3$ (STF), $Sr(Ti_{1-x}Co_x)O_3$ (STC), and $Sr(Ti_{1-x}Cr_x)O_3$ (STCr) were prepared by a conventional mixed oxide sintering method. Detailed target preparation methods are described elsewhere.^{4,8} The films were deposited on single crystal substrates of STO (lattice parameter 0.3905 nm) or $LaAlO_3$ (LAO, measured lattice parameter 0.3786 nm), or on Si coated with YSZ/ CeO_2 buffer layers to enable epitaxial growth of STC, STF, and STCr. The CeO_2 has a lattice parameter of 0.539 nm, which gives a fit to a 0.381 nm perovskite lattice rotated by 45° with respect to the CeO_2 . The YSZ and CeO_2 films were deposited on substrates heated to 800 °C. The laser frequency was 10 Hz, the energy was 400 mJ/pulse, and the fluence at the target was 1.3 J/cm². The oxygen pressure in the chamber during deposition of

TABLE I. Transition-metal ions (d^n) in octahedral oxygen coordinations.

n	Ions ^a	S	Occupancy ^b	Spontaneous spin stabilization along [001] axis
0	Ti^{4+} , V^{5+} , Cr^{6+} , <u>Nb^{5+}</u> , <u>Mo^{6+}</u>	0	$t_{2g}^0 e_g^0$	none (empty d shell)
1	Ti^{3+} , V^{4+} , Cr^{5+} , <u>Nb^{4+}</u> , <u>Mo^{5+}</u>	1/2	$t_{2g}^1 e_g^0$	J-T or S-O stabilization
2	Ti^{2+} , V^{3+} , Cr^{4+} , <u>Nb^{3+}</u> , <u>Mo^{4+}</u>	1	$t_{2g}^2 e_g^0$	J-T or S-O stabilization
3	Cr^{3+} , Mn^{4+}	3/2	$t_{2g}^3 e_g^0$	none (half-filled t_{2g})
4	Cr^{2+} , Mn^{3+} , Fe^{4+} , <u>Ru^{4+}</u> , Mn^{III} , Fe^{IV} , <u>Ru^{IV}</u>	2; 1	$t_{2g}^3 e_g^1$; $t_{2g}^4 e_g^0$	pure J-T stabilization; J-T or S-O stabilization
5	Mn^{2+} , Fe^{3+} , Co^{4+} , <u>Ru^{3+}</u> ; Mn^{II} , Fe^{III} , Co^{IV} , <u>Ru^{III}</u>	5/2; 1/2	$t_{2g}^3 e_g^2$; $t_{2g}^5 e_g^0$	none (half-filled d shell); J-T or S-O stabilization
6	Fe^{2+} , Co^{3+} ; Fe^{II} , Co^{III}	2; 0	$t_{2g}^4 e_g^2$; $t_{2g}^6 e_g^0$	J-T or S-O stabilization; none (filled t_{2g})
7	Co^{2+} , Ni^{3+} ; Co^{II} , Ni^{III}	3/2; 1/2	$t_{2g}^5 e_g^2$; $t_{2g}^6 e_g^1$	J-T or S-O stabilization; pure J-T stabilization
8	Ni^{2+} , Cu^{3+} ; Ni^{II} , Cu^{III}	1; 0 ^d	$t_{2g}^6 e_g^2$; $t_{2g}^6 e_g^2$	none (filled t_{2g} , half-filled e_g); static J-T at low T (filled d_{z^2} , empty $d_{x^2-y^2}$)
9	Cu^{2+}	1/2	$t_{2g}^6 e_g^3$	pure J-T stabilization

^aRoman superscript convention is used to indicate $3d^n$ low-spin configurations, i.e., $\text{Fe}^{\text{III}} \equiv$ low spin Fe^{3+} . Underlined entries are from the $4d^n$ shell.

^bOrbital state occupancies are based on the analysis of Tanabe and Sugano.^{28,29}

^cA degeneracy in the e_g shell can stabilize only a singlet with no first-order orbital angular momentum (pure J-T effect). In the t_{2g} shell an axial distortion can stabilize either the singlet (J-T) or the spin-orbit doublet (S-O). In the absence of an exchange field, or an offsetting external strain, the J-T option is expected to dominate.^{30,31}

^dA special case reported by Goodenough *et al.*,³² where the J-T splitting of the e_g doublet is sufficient to allow a violation of Hund's rule by filling the lower d_{z^2} state and leaving the upper $d_{x^2-y^2}$ available for spin transport.³³

YSZ and CeO_2 was 0.4 and 5 mTorr respectively. In the case of YSZ, the film was deposited at high vacuum for 30 seconds before introducing oxygen to avoid formation of SiO_2 on the Si substrate and to increase adhesion between the YSZ and Si substrate. STF and STC films were usually deposited in vacuum (2×10^{-6} Torr) at temperatures of 650–800 °C and laser fluence of 1.6 to 4 J/cm². The STCr thin films were deposited from single targets made from SrCO_3 , TiO_2 , and Cr_2O_3 powders (Alfa Aesar, 99.97%) at 1.3 J/cm², target-substrate distance of 8 cm, pressure of 2×10^{-6} Torr, and substrate temperature of 650–800 °C. The as-deposited films were cooled down to room temperature at a rate of 5 °C/min in vacuum.

X-ray diffraction (XRD, Rigaku D/MAX-R with $\text{CuK}\alpha$ radiation, $\lambda = 0.15406$ nm) and high-resolution transmission electron microscopy (HR-TEM, JEOL JEM 2010) were used to identify the film structure. Using x-ray reciprocal space mapping, the in-plane structure and strain state were investigated. Two-dimensional XRD (2DXRD) was used to evaluate the in-plane lattice parameter and strain. Magnetic measurements were carried out with superconducting quantum interference device (SQUID) magnetometry and vibrating sample magnetometry (VSM). The magnetic hysteresis loops were obtained after subtracting the diamagnetic substrate signal. X-ray photoelectron spectroscopy (XPS) was measured using a Kratos AXIS Ultra imaging spectrometer with a monochromatic Al $K\alpha$ radiation source and data fitting was obtained by Casa XPS with a Shirley background. The accuracy in the peak energies was 0.25 eV. The composition was measured by wavelength dispersive x-ray spectroscopy (WDS), which showed that a target with $\text{Fe}:\text{Ti} = 0.5:0.5$ produced a film with $\text{Fe}:\text{Ti} = 0.45:0.55$. Similarly, the $\text{Co}:\text{Ti}$ ratio in STC and the $\text{Cr}:\text{Ti}$ ratio in STCr were smaller than the ratios in the targets.

The data below are described with reference to the measured film compositions.

IV. RESULTS AND DISCUSSION

A. Fe-substituted STO

Fe substituted SrTiO_3 has been the focus of interest for various applications such as electrochemical electrodes, gas sensors, and magnetic devices,^{4,34,35} and the magnetic behavior of $\text{La}_{0.35}\text{Sr}_{0.65}\text{Ti}_{1-x}\text{Fe}_x\text{O}_3$ ($0.1 \leq x \leq 0.4$) thin films³⁶ and bulk SrTiO_3 implanted with Fe³⁷ has been reported. $\text{Sr}(\text{Ti}_{1-x}\text{Fe}_x)\text{O}_3$ ($0 \leq x \leq 1$) exhibits a continuous solid solution between SrTiO_3 and antiferromagnetic SrFeO_3 .³⁸ We found previously⁸ that STF thin films grown on LAO had a highly anisotropic magnetic hysteresis, with a uniaxial out-of-plane anisotropy, large coercivity, and saturation magnetic moment of $\sim 0.5 \mu_B/\text{Fe}$.

80-nm-thick films STF deposited on $\text{CeO}_2/\text{YSZ}/\text{Si}$ at 2×10^{-6} Torr grew as polycrystalline films, as single crystal films or as “double-epitaxial” films depending on the Fe content, similar to results reported earlier.⁴ Polycrystalline films showed (100), (111), and (110) peaks and no epitaxial relation between the film and the substrate. Single-crystal films had a (100) orientation with a 45°-rotated epitaxy on the CeO_2 . Double-epitaxial films consisted of a (100) STF matrix containing (110) pyramid-shaped crystals. Both the (100) and (110) regions were epitaxial with respect to the CeO_2 . It is believed that the (110) regions are formed to reduce the film strain.⁴

As the Fe content increased, the film microstructure progressed from polycrystalline (seen at $x = 0$) to double-epitaxial for low Fe contents ($0.04 \leq x \leq 0.13$), to single crystal for $0.34 \leq x \leq 0.36$. (110) peaks reappeared

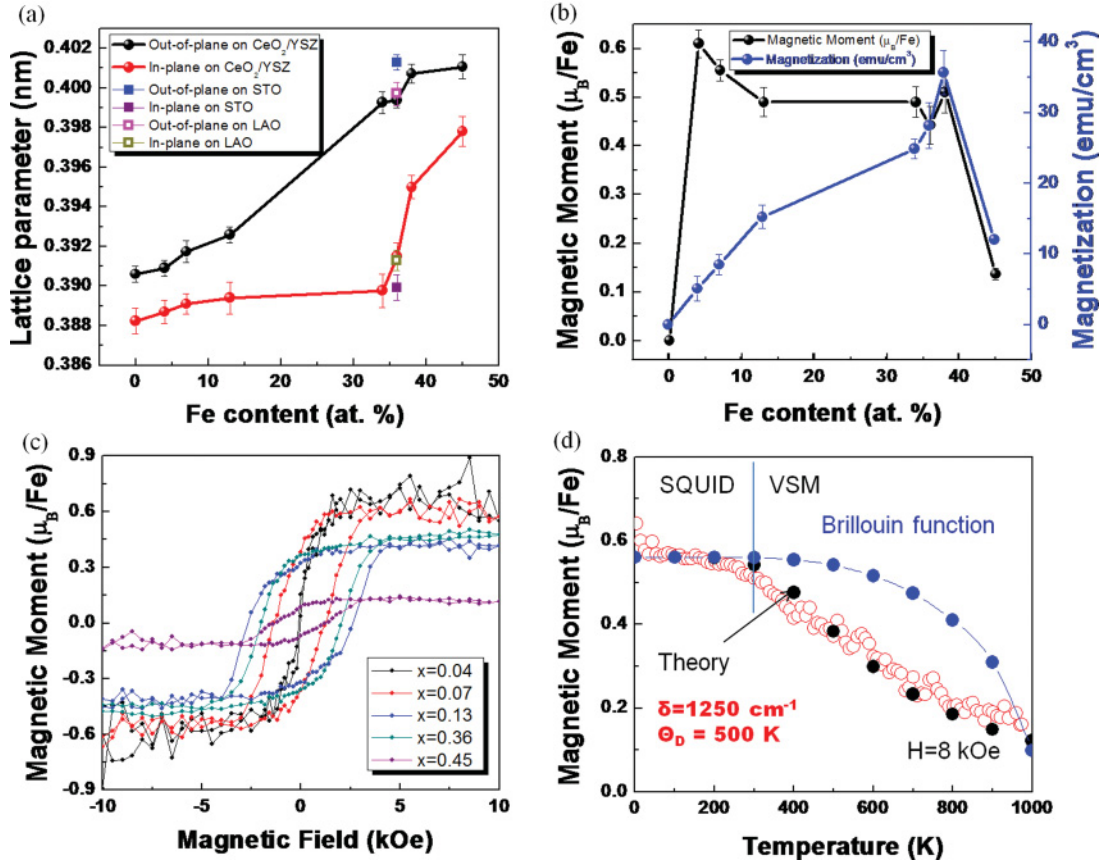


FIG. 2. (Color online) (a) Lattice parameter, (b) saturation magnetization, and (c) hysteresis loops of $\text{Sr}(\text{Ti}_{1-x}\text{Fe}_x)\text{O}_{3-\delta}$ thin films as a function of Fe content. (d) The in-plane magnetization-temperature curve of a film with $x = 0.36$ measured at 8 kOe. Fits to the magnetoelastic model and the Brillouin function are included. These converge at low temperature.

at $x = 0.38$. The competition between (100) and (110) orientations depends on the lattice mismatch, which favors (100), and on the polarity of the CeO_2 , which favors (110) growth.⁴ There were no diffraction peaks from iron or iron oxide for $x < 0.45$ but a small peak at 43.4° presumed to be from iron oxide appeared at $x = 0.45$ and above. The out-of-plane lattice parameter calculated from the (100)-peak position increases monotonically up to $x = 0.45$, see Fig. 2(a).

The in-plane lattice parameter of STF films increased slightly with Fe content up to $x = 0.34$, then increased more rapidly. Despite some strain relaxation, all the films were tetragonally distorted (the out-of-plane lattice parameter exceeds the in-plane lattice parameter, i.e., $c/a > 1$) and under in-plane compression due to epitaxial growth on the CeO_2 . As an example, a film with $x = 0.36$ had an in-plane lattice parameter of 0.3915 nm and an out-of-plane lattice parameter of 0.3994 nm giving a unit cell volume of 0.06121 nm^3 , which exceeded that of the STO film, 0.05887 nm^3 . The increase of unit cell volume with x is attributed to the existence of low-valence-state Fe ions, which have a relatively large ionic radius compared to Ti^{4+} (the ionic radius of Fe^{4+} is 0.0585 nm, of Fe^{3+} (high spin) is 0.0645 nm, of Fe^{2+} (high spin) is 0.0780 nm, and of Ti^{4+} is 0.0605 nm) and expand the STO lattice. XPS on films with $x = 0.04 - 0.45$ showed that Fe ions existed as a mixed-valence state including +2, +3, and +4, with the lower-valence ions present for charge balance in the oxygen-deficient films.

Figure 2(b) shows the saturation magnetization of the 80-nm-thick STF films. The pure STO film was diamagnetic and the STF with $x = 0.04$ film had almost zero coercivity and anisotropy both at room temperature and at 5 K, and a high-field moment of $\sim 0.6 \mu_B/\text{Fe}$. Films with $0.07 \leq x \leq 0.38$ exhibited room-temperature ferromagnetic hysteresis, Fig. 2(c), with an out-of-plane easy axis and saturation magnetizations of around $0.5 \mu_B/\text{Fe}$, and a gradually increasing out-of-plane coercivity. The saturation moment, M_s , decrease above $x = 0.45$ is attributed to the increasing dominance of antiferromagnetic exchange interactions.

Figure 2(d) shows in-plane magnetization vs. temperature for samples with $x = 0.36$ at an applied field of 8 kOe, measured from 5 to 973 K. The $M(T)$ is fitted using a model for magnetoelastic spin ordering²⁶ in which $M(T)$ is determined by a Boltzmann ratio giving the probability of occupation of the upper and lower split orbital states. The saturated $M_s(T)$ contour is non-Brillouin and is given by

$$M_s(T) = M_s(0) \tanh \left[\frac{(\delta(0) \tanh(\Theta_D/2T))}{2kT} \right], \quad (1)$$

where Θ_D is the Debye temperature and δ is the orbital splitting, labeled δ_e for e_g states and δ_t for t_{2g} states, as defined in Fig. 1. The model was developed to explain the magnetoelastic behavior of dilute Cr^{2+} (d^4) in In_2O_3 ^{39,40} in which the splitting of e_g was based on a cooperative J-T effect enhanced by a tensile strain that created $\delta_e(0) = 1000 \text{ cm}^{-1}$,

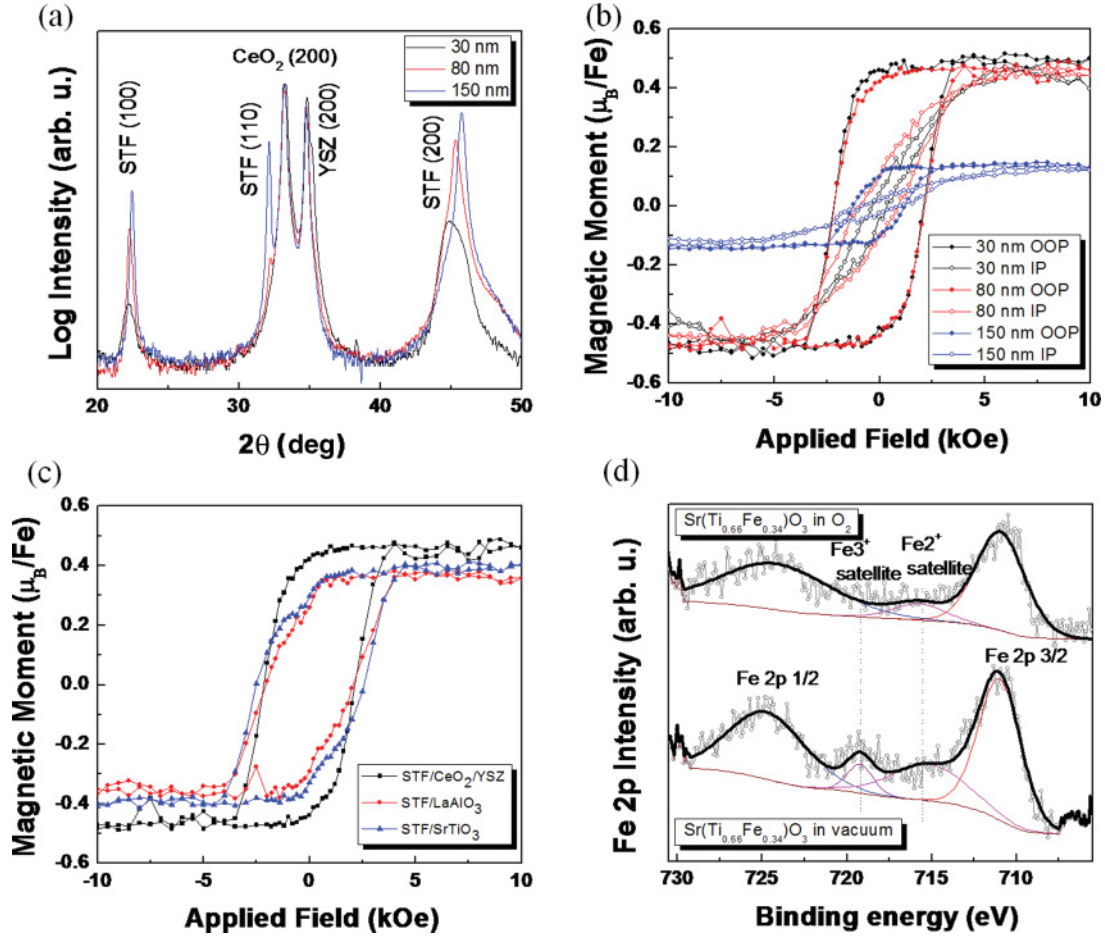


FIG. 3. (Color online) (a) XRD patterns and (b) magnetic hysteresis loops of $\text{Sr}(\text{Ti}_{0.64}\text{Fe}_{0.36})\text{O}_{3-\delta}$ thin films as a function of thickness. (c) Hysteresis loops of $\text{Sr}(\text{Ti}_{0.64}\text{Fe}_{0.36})\text{O}_{3-\delta}$ grown on different substrates. (d) XPS spectra of Fe $2p$ in $\text{Sr}(\text{Ti}_{0.66}\text{Fe}_{0.34})\text{O}_{3-\delta}$ thin films deposited at high vacuum and in an oxygen atmosphere.

and a value of $\Theta_D = 500$ K was taken. The fit to the STF sample is shown for $\delta_i(0) = 1250 \text{ cm}^{-1}$ from Fig. 1(b) for Fe^{IV} and $\Theta_D = 500$ K, with $M_s(0) = 0.56 \mu_B/\text{Fe}$. The value for $\delta(0)$ is consistent with estimates from crystal-field distortions and from fits to other oxide materials²³ and the value of Θ_D is typical for transition-metal oxide lattices.²⁶ For comparison, a fit to the Brillouin function was also made to match the data at 0 and 1000 K. It is clear that the Brillouin function fits very poorly to the data compared to the magnetoelastic model.

Figures 3(a) and 3(b) show the effects of film thickness on the x-ray diffraction and magnetic hysteresis for films with $x = 0.36$. The 30 and 80 nm thick films show (100) peaks with little or no (110) peak, while the 150 nm film shows a strong (110) peak as the double-epitaxial microstructure develops. The out-of-plane lattice parameters for 30, 80, and 150 nm thickness films were 0.4001, 0.3994, and 0.3976 nm, respectively, showing that the compressive in-plane strain changes little between the 30 nm and 80 nm films, but decreases as the film thickness increases to 150 nm. This correlates with the trend in anisotropy. The 30 and 80 nm thick films have similar hysteresis loops though the anisotropy is slightly weaker for the 80 nm film, and the 150 nm film has a much lower anisotropy. The 150 nm film also has a much lower magnetic moment. The reason for this is not fully understood

but similar behavior was observed in other samples, and thickness-dependent magnetization attributed to changes in strain has been observed in other oxide materials.⁴¹ It is also possible that the magnetization reduction could be caused by inhomogeneous Fe distribution,⁴² since higher-Fe regions have lower magnetization.

Figure 3(c) compares films on different substrates. Films of (100) single-crystal STF with $x = 0.36$ on $\text{CeO}_2/\text{YSZ}/\text{Si}$, LAO (100), and STO (100) substrates all show a strong out-of-plane anisotropy. In each case the films are compressively strained in plane with out-of-plane lattice parameters of 0.3994, 0.3997, and 0.4013 nm and in-plane lattice parameters of 0.3915, 0.3913, and 0.3899 nm, respectively [(see Fig. 2(a)], giving unit cell volumes of 0.06122, 0.06120, and 0.06101 nm^3 , respectively. The films are tetragonally distorted with a c/a ratio of 1.020, 1.021, and 1.029, respectively. The film on STO would be expected to have lowest strain due to the higher substrate lattice parameter but it actually shows a higher tetragonality, and its smaller unit cell volume may indicate a different oxygen stoichiometry and populations of Fe ions. Any reduction of low-spin Fe^{4+} ions to non-magnetoelastic Fe^{3+} would diminish the observed magnetic behavior. This indicates that lattice mismatch is not the only factor influencing the strain state, which may also be

affected by the substrate polarity or by the thermal expansion mismatch, which could change, for example, the number of misfit dislocations generated during film growth or the onset of the double-epitaxial microstructure. However, the presence of both a strong magnetic anisotropy and a tetragonal distortion in the samples is evident.

Films deposited in oxygen show significantly different behavior compared to the vacuum-deposited samples already discussed. Films grown in 5 mTorr oxygen with $x = 0.34$ and 0.36 had a paramagnetic response both at room temperature and low temperatures (5 K) and no remanence. XPS data for $x = 0.34$ are given in Fig. 3(d). The Fe $2p_{2/3}$ and $2p_{1/2}$ doublets occur at 711.5 and 725.3 eV for vacuum-deposited thin films and 711.4 and 725.0 eV for films grown in oxygen, respectively. These peaks appear at a higher binding energy compared to measurements on Fe_2O_3 in which Fe is trivalent.^{43,44} The peak shift is 0.4 eV for the vacuum-deposited film and 0.5 eV for the oxygen-deposited film. This peak shift is evidence for the existence of Fe^{4+} ^{43,45,46} and the higher shift for the oxygen-deposited film shows a greater proportion of Fe^{4+} , as expected. Other elements such as Sr 3d, Ti 2p, O 1s, and C 1s for calibration showed the same binding energies for the two samples. The oxygen-deposited film also has smaller satellite peaks indicating a greater amount of Fe^{4+} .

XRD indicates that the oxygen-deposited films have smaller lattice parameters and unit cell volumes. For $x = 0.34$, the out-of-plane lattice parameter was 0.3919 nm compared to 0.3993 nm for the vacuum-deposited film, and the in-plane lattice parameter was 0.3869 nm ($c/a = 1.01$) compared to 0.3898 nm. In addition, a (111) peak appeared in the film deposited in oxygen. The unit cell volumes of STF films deposited in oxygen, 0.05866 and 0.05873 nm³ for $x = 0.34$ and 0.36 , are almost the same as those of bulk STF, 0.05877 and 0.05873 nm³ for $x = 0.34$ and 0.36 predicted from Vegard's law. The paramagnetic behavior of oxygen-deposited films is assumed to be a result of the low strain state in the film and/or the presence of antiferromagnetic coupling between the dominant Fe^{4+} ions.

Taken together these data indicate an important role for magnetoelastic effects in STF films with a mixed Fe valence over a range of compositions and substrates. A strong out-of-plane anisotropy is consistent with the presence of magnetoelastic Fe ions and the compressive in-plane strain in the films.

B. Co-substituted STO

Similar to Fe-substituted STO, Co has a full range of solubility in the STO lattice in bulk.^{47,48} We previously reported the magnetic properties of $\text{Sr}(\text{Ti}_{1-x}\text{Co}_x)\text{O}_{3-\delta}$ epitaxial thin films on LAO, where δ represents the oxygen deficiency, which showed room-temperature magnetism and strong out-of-plane magnetic anisotropy at Co concentrations of $x = 0.07$ – 0.37 .⁴⁹ Co-doped $\text{La}_{1-x}\text{Sr}_x\text{TiO}_3$ with low Co content has been studied by several groups. Intrinsic^{50,51} and metal-cluster-induced⁵² ferromagnetism were both reported, as well as significant in-plane magnetoelastic anisotropy in epitaxial films grown on an orthorhombic substrate.⁵¹

In room-temperature ferromagnetic $\text{Sr}(\text{Ti}_{0.77}\text{Co}_{0.23})\text{O}_{3-\delta}$ ($x = 0.23$) films on LAO, XPS showed that Co is in a

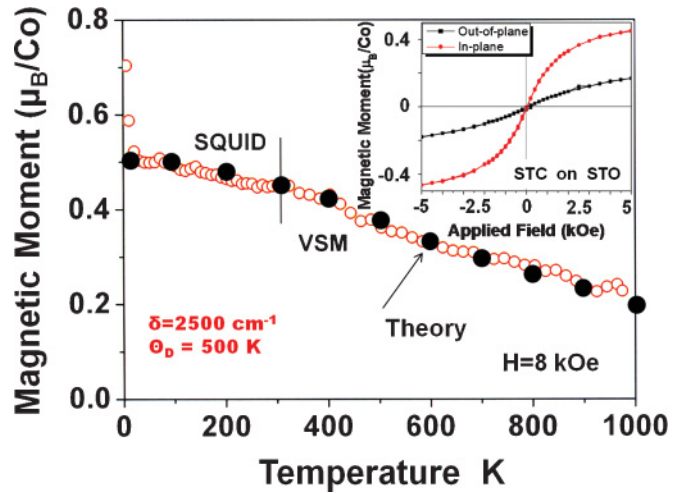


FIG. 4. (Color online) The saturation magnetization-temperature curve of a $\text{Sr}(\text{Ti}_{0.77}\text{Co}_{0.23})\text{O}_{3-\delta}$ film on LAO at 8 kOe with the magnetic field applied out-of-plane, with a fit to Eq. (1). The inset (see Ref. 49) shows the room temperature hysteresis loops.

mixed-valence state of Co^{2+} , Co^{3+} , and Co^{4+} , although the technique does not allow unambiguous determination of the relative fractions of the species.⁴⁹ As listed in Table I for the various Co ions, which could be present in STF, only Co^{4+} and low-spin Co^{3+} ions are not magnetoelastic due to the half-filled d shell or filled t_{2g} shell, respectively.

An STF film with $x = 0.23$ grown on LAO at 3.5×10^{-6} Torr base pressure had out-of-plane and in-plane lattice parameters of 0.3993 nm and 0.3914 nm respectively, i.e., $c/a = 1.02$, with in-plane compressive strain. This sample showed a weak out-of-plane anisotropy and low coercivity. The $M_s(T)$ curve decreased almost linearly with increasing temperature up to 1000 K, as shown in Fig. 4. The curve was fitted using the model for magnetoelastic spin ordering²⁶ using a Debye temperature of $\Theta_D = 500$ K (Ref. 53) and J-T energy $\delta_t(0) = 2500$ cm⁻¹. The data are matched very poorly by a Brillouin function (not shown), similarly to the STF case in Fig. 2(d).

Lowering the base pressure during growth to 2.5×10^{-6} Torr, greatly increased the coercivity and the out-of-plane anisotropy while a sample grown on STO at the same time as the sample of Fig. 4 had an out-of-plane lattice parameter of 0.3998 nm and a weak in-plane anisotropy.⁴⁹ The differences between the samples are assumed to result from changes in the populations of oxygen vacancies and Co ions under different fabrication conditions, and changes in strain state. Since different Co ions can contribute positive or negative magnetoelastic behavior, a characterization of the Co ion concentrations as well as the c/a ratio is needed to explain the trends in magnetic anisotropy.

C. Cr-substituted STO

Chromium is an interesting substituent because it can have various oxidation states, i.e., Cr^{2+} , Cr^{3+} , Cr^{4+} , and Cr^{6+} . Cr^{4+} is present in ferromagnetic CrO_2 but this material is metastable and difficult to synthesize, requiring high oxygen pressure.^{54,55} The 3+ oxidation state is the most stable but

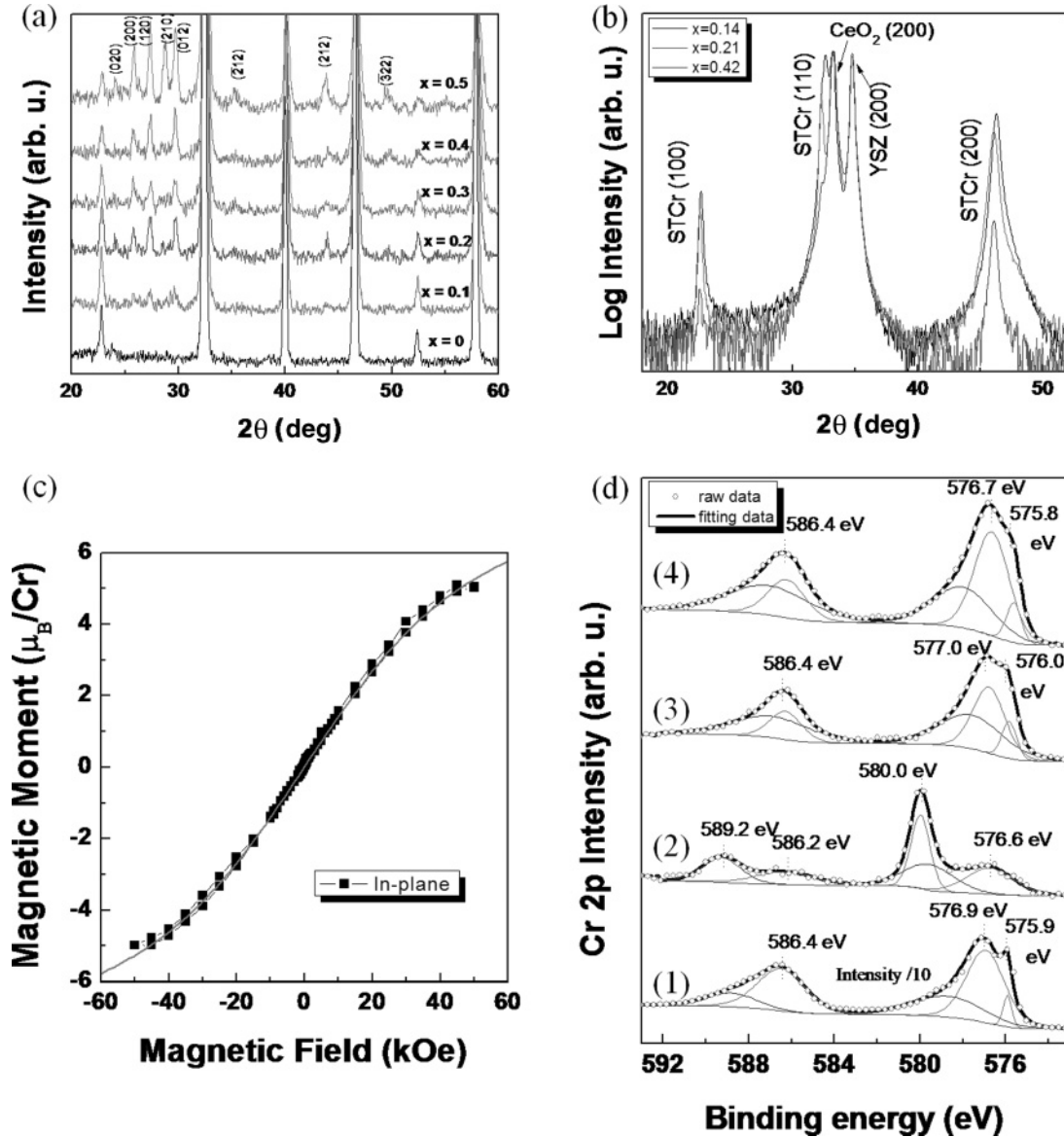


FIG. 5. (Color online) (a) XRD patterns of $\text{Sr}(\text{Ti}_{1-x}\text{Cr}_x)\text{O}_3$ powders calcined at 1250 °C for 3 hours. (b) XRD patterns of $\text{Sr}(\text{Ti}_{1-x}\text{Cr}_x)\text{O}_{3-\delta}$ thin films deposited at 700 °C on CeO_2/YSZ buffered Si substrate. (c) In-plane magnetization of STCr film with $x = 0.21$ measured by SQUID at 5 K. (d) XPS of Cr 2p in (1) Cr_2O_3 powder, (2) $\text{Sr}(\text{Ti}_{0.7}\text{Cr}_{0.3})\text{O}_3$ powder calcined at 1250 °C, (3) $\text{Sr}(\text{Ti}_{0.79}\text{Cr}_{0.21})\text{O}_3$, and (4) $\text{Sr}(\text{Ti}_{0.58}\text{Cr}_{0.42})\text{O}_3$ films.

has no magnetoelastic effect as shown in Table I.³³ Cr-doped SrTiO_3 exhibits a bistable resistance and has been considered as a candidate for memory devices^{56,57} or photocatalysts in wastewater treatment and hydrogen generation.^{58,59} In terms of its magnetic properties, Inaba *et al.* found weak ferromagnetic behavior and a large negative magnetoresistance by controlling the carrier density in SrTiO_3 by substitution of La for Sr and the magnetic properties by substitution of Cr for Ti.⁶⁰ They suggested that ferromagnetism arises from carrier-mediated (double) exchange interactions between the Cr ions. Other groups showed no ferromagnetism in transition metal (Cr, Co, Fe, and Mn) and Nb co-doped SrTiO_3 films grown by PLD, though the conductivity improved dramatically by donor doping with Nb.⁶¹ However, there is little work on the magnetic and magnetoelastic properties of Cr-doped SrTiO_3 films.

Figure 5 compares the structure of the STCr as bulk ceramic material with that of thin films. Figure 5(a) shows the XRD patterns of $\text{Sr}(\text{Ti}_{1-x}\text{Cr}_x)\text{O}_3$ powders calcined at 1250 °C. All the powders showed a perovskite phase with additional SrCrO_4 phases (marked with round brackets) that increased as the Cr content increased. The solubility limit of Cr in the Ti site is less than 10 at.%, and excess Cr forms SrCrO_4 in which chromium exists as Cr^{6+} . The lattice parameter of the STCr phase decreased as Cr was added. The lattice parameters of the perovskite phases in the SrTiO_3 , $\text{Sr}(\text{Ti}_{0.9}\text{Cr}_{0.1})\text{O}_3$, $\text{Sr}(\text{Ti}_{0.8}\text{Cr}_{0.2})\text{O}_3$, $\text{Sr}(\text{Ti}_{0.7}\text{Cr}_{0.3})\text{O}_3$, $\text{Sr}(\text{Ti}_{0.6}\text{Cr}_{0.4})\text{O}_3$, and $\text{Sr}(\text{Ti}_{0.5}\text{Cr}_{0.5})\text{O}_3$ targets made from the calcined powders were 0.3905, 0.3898, 0.3896, 0.3893, 0.3890, and 0.3885 nm, respectively. The continued decrease in lattice parameter beyond the solubility limit may be a result of Cr^{3+} substitution into the Sr^{2+} site.⁶²

$\text{Sr}(\text{Ti}_{1-x}\text{Cr}_x)\text{O}_{3-\delta}$ thin films with $x = 0.14$ and above, deposited on CeO_2/YSZ buffered Si at 700°C , grew either as single-crystal epitaxial (100) films or as a double-epitaxial film consisting of (110) nanopillars embedded in a (100) matrix, similar to the growth of STF.^{4,8} As in previous reports,^{4,63} films with $x = 0$ and $x = 0.10$ were polycrystalline (not shown here). The XRD patterns of STCr with $x = 0.14, 0.21$, and 0.42 in Fig. 5(b) showed no evidence for chromium metal or chromium oxide impurities. As the Cr content increased, the (110) peaks decreased and shifted to lower angles, corresponding to an increase in the out-of-plane lattice parameters of STCr films, which were $0.3901, 0.3911, 0.3921, 0.3934$, and 0.3937 nm for $x = 0, 0.10, 0.14, 0.21$, and 0.42 , respectively. These trends are the same as for the STF, and imply an in-plane compression in the films, but unlike STF, none of the STCr thin films deposited at $650\sim 800^\circ\text{C}$ showed magnetic properties at room temperature. SQUID measurements showed Cr paramagnetism that became evident only at temperatures of a few K [see Fig. 5(c)].

The lack of high-temperature ferromagnetism and anisotropy in STCr suggests that the chromium ions are not present as magnetoelastic Cr^{4+} ions in a strained lattice. Figure 5(d) shows high-resolution XPS spectra of the Cr $2p$ peak for commercial Cr_2O_3 powder, $\text{Sr}(\text{Ti}_{0.7}\text{Cr}_{0.3})\text{O}_3$ powder calcined at 1250°C (both are included for reference), and the STCr films with $x = 0.21$ and 0.42 . Other elements such as Sr, Ti, and O measured for the four samples showed almost the same binding energies. In the case of the Cr_2O_3 powder, there are two Cr $2p$ doublets: Cr $2p_{3/2}$ at binding energies of 576.9 and 575.9 eV, and Cr $2p_{1/2}$ at binding energy of 586.5 eV. The splitting of Cr $2p_{3/2}$ is attributed to the multiplet interaction.⁶⁴ The $\text{Sr}(\text{Ti}_{0.7}\text{Cr}_{0.3})\text{O}_3$ powder calcined at 1250°C shows Cr in dual valence states of $3+$ and $6+$ but Cr^{6+} is dominant. Two peaks at binding energies of 580.0 and 589.2 eV are due to $2p_{3/2}$ and $2p_{1/2}$ of Cr^{6+} .⁶⁵ The small peaks around 576.6 and 586.2 eV show the presence of a small amount of Cr^{3+} .

The STCr thin films show qualitatively different spectra compared to the $\text{Sr}(\text{Ti}_{0.7}\text{Cr}_{0.3})\text{O}_3$ powder but similar to the Cr_2O_3 powder, suggesting that Cr^{3+} is the dominant ion. This is consistent with the increase in lattice parameter with Cr content, which results from the larger ionic radius of Cr^{3+} (0.0615 nm) compared to Ti^{4+} (0.0605 nm). Cr^{3+} like Cr^{6+} has no magnetoelastic properties, so its magnetization is not stabilized by magnetoelastic effects, precluding the existence of a strong anisotropy or high-temperature magnetism.

V. CONCLUSIONS

Magnetoelastic effects can be an important contributor to the magnetic behavior of transition-metal-substituted oxides, particularly in thin films, where lattice mismatch, thermal mismatch and/or bombardment, and coalescence during growth typically lead to high biaxial states of stress. Magnetoelastic contributions are associated with characteristic magnetic behavior, including the presence of significant anisotropy dependent on the strain state even at low concentrations of the transition metal, a high Curie temperature, and a relation between magnetic moment and temperature that does not follow the Brillouin function. These characteristics can serve as indicators for magnetoelastic behavior, and differ qualitatively from the behavior expected in systems dominated by exchange or by metal clusters.

Magnetoelastic effects have been analyzed here in the case of octahedrally coordinated transition metal ions in the B site of the perovskite lattice. Data for (100)-oriented Fe, Co, and Cr-substituted SrTiO_3 are consistent with a dominating effect of lattice mismatch strains on the magnetic properties, in which the majority Co and Fe ions are magnetoelastic whereas the Cr ions are not. Similar principles can be developed for other host lattices by considering the behavior of transition metal ions in other sites, such as tetrahedral sites, and for different directions of strain.

An understanding of magnetoelastic effects is key to the development of transition-metal oxides for magnetic, spintronic, or multiferroic devices where high-temperature magnetization is required. By selecting appropriate magnetoelastic ions, host lattice, crystal orientation, and substrate and by controlling the valence state of ions through the deposition conditions or by substitution of codopants, the magnetic properties of the material can be tailored. Magnetoelastic effects also provide the possibility of modulating the magnetic properties by changing the film strain, for example, piezoelectrically, enabling electrical control of magnetic behavior.

ACKNOWLEDGMENTS

This work was supported by NSF Division of Materials Research and Samsung. L. B. acknowledges an Intel Fellowship and P. J. acknowledges support from the Chinese Scholarship Council.

*caross@mit.edu

¹Y. Matsumoto, M. Murakami, T. Shono, T. Hasegawa, T. Fukumura, M. Kawasaki, P. Ahmet, T. Chikyow, S. Koshihara, and H. Koinuma, *Science* **291**, 854 (2001).

²P. Sharma, A. Gupta, K. V. Rao, F. J. Owens, R. Sharma, R. Ahuja, J. M. O. Guillen, V. Johansson, and G. A. Gehring, *Nat. Mater.* **2**, 673 (2003).

³K. A. Griffin, A. B. Pakhomov, C. M. Wang, S. M. Heald, and K. M. Krishnan, *Phys. Rev. Lett.* **94**, 157204 (2005).

⁴H.-S. Kim, L. Bi, H. Paik, D.-J. Yang, Y. C. Park, G. F. Dionne, and C. A. Ross, *Nano Lett.* **10**, 597 (2010).

⁵L. A. Errico, M. Rentería, and M. Weissmann, *Phys. Rev. B* **72**, 184425 (2005).

⁶B. Vodonko, Y. Zheng, F. Vidal, D. Demaille, and V. H. Etgens, *Appl. Phys. Lett.* **90**, 062510 (2007).

⁷Z. D. Dohčević-Mitrović, N. Paunović, M. Radović, Z. V. Popović, B. Matović, B. Cekić, and V. Ivanovski, *Appl. Phys. Lett.* **96**, 203104 (2010).

⁸H.-S. Kim, L. Bi, G. F. Dionne, and C. A. Ross, *Appl. Phys. Lett.* **93**, 092506 (2008).

⁹Y. Belghazi, G. Schmerber, S. Colis, J. L. Rehspringer, and A. Dinia, *Appl. Phys. Lett.* **89**, 122504 (2006).

- ¹⁰J. H. Park, M. G. Kim, H. M. Jung, and S. Ryu, *Appl. Phys. Lett.* **84**, 1338 (2004).
- ¹¹S. Ramachandran, A. Tiwari, and J. Narayan, *Appl. Phys. Lett.* **84**, 5255 (2004).
- ¹²K. Rode, A. Anane, R. Mattana, J.-P. Contour, O. Durand, and R. LeBourgeois, *J. Appl. Phys.* **93**, 7676 (2003).
- ¹³J. M. D. Coey, M. Venkatesan, and C. B. Fitzgerald, *Nat. Mater.* **4**, 173 (2005).
- ¹⁴M. Venkatesan, C. B. Fitzgerald, J. G. Lunney and J. M. D. Coey, *Phys. Rev. Lett.* **93**, 177206 (2004).
- ¹⁵J. C. Slater, *Phys. Rev.* **49**, 537 (1936).
- ¹⁶J. B. Goodenough, *Magnetism and the Chemical Bond* (Interscience, John Wiley, New York 1963), Chap. III.
- ¹⁷G. F. Dionne, *Magnetic Oxides* (Springer, New York, 2009), Chap. 1.
- ¹⁸J. C. Slonczewski, *Phys. Rev.* **101**, 1341 (1958).
- ¹⁹G. F. Dionne and R. G. West, *Appl. Phys. Lett.* **48**, 1488 (1986).
- ²⁰Q. Gan, R. A. Rao, C. B. Eom, J. L. Garrett, and M. Lee, *Appl. Phys. Lett.* **72**, 978 (1998).
- ²¹A. Grutter, F. Wong, E. Arenholz, M. Liberati, A. Vailionis, and Y. Suzuki, *Appl. Phys. Lett.* **96**, 082509 (2010).
- ²²G. F. Dionne, *IEEE Trans. Magn.* **47**, 272 (2011).
- ²³H. L. Schlafer and G. Gliemann, *Basic Principles of Ligand Field Theory* (Wiley-Interscience, New York, 1969).
- ²⁴G. F. Dionne and J. B. Goodenough, *Mater. Res. Bull.* **7**, 749 (1972).
- ²⁵G. F. Dionne, *Magnetic Oxides* (Springer, New York, 2009), p. 76.
- ²⁶G. F. Dionne, *J. Appl. Phys.* **101**, 09C509 (2007).
- ²⁷J. B. Goodenough, A. Wold, N. Menyuk, and R. J. Arnett, *Phys. Rev.* **124**, 373 (1961).
- ²⁸Y. Tanabe and S. Sugano, *J. Phys. Soc. Jpn.* **9**, 753 (1954).
- ²⁹D. S. McClure, *Solid State Physics* **9**, 399 (1959).
- ³⁰J. B. Goodenough, *Magnetism and the Chemical Bond* (Interscience, John Wiley, New York 1963), pp. 213.
- ³¹G. F. Dionne, *J. Appl. Phys.* **67**, 4561 (1990).
- ³²J. B. Goodenough, G. Demazeau, M. Pouchard, and P. Hagenmuller, *Solid State Chem.* **8**, 1814 (1973).
- ³³G. F. Dionne, *J. Appl. Phys.* **79**, 5172 (1996).
- ³⁴A. A. L. Ferreira, J. C. C. Abrantes, J. R. Jurado, and J. R. Frade, *Solid State Ionics* **135**, 761 (2000).
- ³⁵W. Jung and H. L. Tuller, *Solid State Ionics* **180**, 843 (2009).
- ³⁶G. W. Leung, M. E. Vickers, T. Fix, and M. G. Blamire, *J. Phys.: Cond. Matter* **21**, 426003 (2009).
- ³⁷S. Kazan, A. G. Şale Ju., I. Gatiatova, V. F. Valeev, R. I. Khaibullin, and F. A. Mikailzade, *Solid State Commun.* **150**, 219 (2010).
- ³⁸S. Srinath, M. M. Kumar, K. Sahner, M. L. Post, M. Wickles, R. Moos, and H. Srikanth, *J. Appl. Phys.* **99**, 08S904 (2006).
- ³⁹J. Philip, A. Punnoose, B. I. Kim, K. M. Reddy, S. Layne, J. O. Holmes, B. Satpati, P. R. Leclair, T. S. Santos, and J. S. Moodera, *Nat. Mater.* **5**, 298 (2006).
- ⁴⁰G. F. Dionne and H.-S. Kim, *J. Appl. Phys.* **103**, 07B333 (2008).
- ⁴¹S. H. Lim, M. Murakami, W. L. Sarney, S. Q. Ren, A. Varathatajan, V. Nagarajan, S. Fujino, M. Wuttig, I. Takeuchi, and L. G. Salamanca-Riba, *Adv. Funct. Mater.* **17**, 2594 (2007).
- ⁴²H.-S. Kim, L. Bi, D. H. Kim, D.-J. Yang, Y. J. Choi, J. W. Lee, J. K. Kang, Y. C. Park, G. F. Dionne, and C. A. Ross, *J. Mater. Chem.* **21**, 10364 (2011).
- ⁴³A. E. Bocquet, A. Fujimori, T. Mizokawa, T. Saitoh, H. Namatame, S. Suga, N. Kimizuka, Y. Takeda, and M. Takano, *Phys. Rev. B* **45**, 1561 (1992).
- ⁴⁴X. Qu, N. Kobayashi, and T. Komatsu, *ACS NANO* **4**, 1732 (2010).
- ⁴⁵H. Kanatani, H. Kume, and T. Matsui, *J. Appl. Phys.* **105**, 07D907 (2009).
- ⁴⁶T. Matsui, E. Taketani, R. Sato, and K. Morii, *J. Phys. D: Appl. Phys.* **40**, 6066 (2007).
- ⁴⁷S. Malo and A. Maignan, *Inorg. Chem.* **43**, 8169 (2004).
- ⁴⁸C. Pascanuta, N. Dragoeb, and P. Berthet, *J. Magn. Magn. Mater.* **6**, 305, (2006).
- ⁴⁹L. Bi, H.-S. Kim, G. F. Dionne, and C. A. Ross, *New J. Phys.* **12**, 043044 (2010).
- ⁵⁰G. Herranz, R. Ranchal, M. Bibes, H. Jaffres, E. Jacquet, J. L. Maurice, K. Bouzehouane, F. Wyczisk, E. Tafrá, M. Basletic, A. Hamzic, C. Colliex, J. P. Contour, A. Barthelemy, and A. Fert, *Phys. Rev. Lett.* **96**, 027207 (2006).
- ⁵¹T. Fix, M. Liberati, H. Aubriet, S.-L. Sahonta, R. Bali, C. Becker, D. Runch, J. L. MacManus-Driscoll, E. Arenholz, and M. G. Blamire, *New J. Phys.* **11**, 073042 (2009).
- ⁵²S. X. Zhang, W. Yu, S. B. Ogale, S. R. Shinde, D. C. Kundaliya, W. K. Tse, S. Y. Young, J. S. Higgins, L. G. Salamanca-Riba, M. Herrera, L. F. Fu, N. D. Browning, R. L. Greene, and T. Venkatesan, *Phys. Rev. B* **76**, 085323 (2007).
- ⁵³M. Ahrens, R. Merkle, B. Rahmati, and J. Maier, *Physica B* **393**, 239 (2007).
- ⁵⁴H. A. Bullen and S. J. Garrett, *Chem. Mater.* **14**, 243 (2002).
- ⁵⁵E. Castillo-Martínez, A. M. Arévalo-López, R. Ruiz-Bustos, and M. A. Alarion-Franco, *Inorg. Chem.* **47**, 8526 (2008).
- ⁵⁶M. Janousch, G. I. Meier, U. Staub, B. Delley, S. F. Karg, and B. P. Andreasson, *Adv. Mater.* **19**, 2232 (2007).
- ⁵⁷A. Beck, J. G. Bednorz, Ch. Gerber, C. Rossel, and D. Widmer, *Appl. Phys. Lett.* **77**, 139 (2000).
- ⁵⁸J. W. Liu, G. Chen, Z. H. Li, and Z. G. Zhang, *J. Solid State Chem.* **179**, 3704 (2006).
- ⁵⁹D. Wang, J. Ye, T. Kako, and T. Kimura, *J. Phys. Chem. B* **110**, 15824 (2006).
- ⁶⁰J. Inaba and T. Katsufuji, *Phys. Rev. B* **72**, 052408 (2005).
- ⁶¹S. X. Zhang, S. B. Ogale, D. C. Kundaliya, L. F. Fu, N. D. Browning, S. Dhar, W. Ramadan, J. S. Higgins, R. L. Greene, and T. Venkatesan, *Appl. Phys. Lett.* **89**, 012501 (2006).
- ⁶²D. Wang, J. Ye, T. Kako, and T. Kimura, *J. Phys. Chem. B* **110**, 15824 (2006).
- ⁶³T. Yamada, N. Wakiya, K. Shinozaki, and N. Mizutani, *Appl. Phys. Lett.* **83**, 4517 (2003).
- ⁶⁴A. R. Pratt and N. S. McIntyre, *Surf. Interface Anal.* **24**, 529 (1996).
- ⁶⁵B. V. Christ, *Handbooks of Monochromatic XPS spectra* (XPS International, California, 1999), Vol. 2, pp. 86–100.